Characterization of Subpicosecond Pulses Based on Temporal Interferometry With Real-Time Tracking of Higher Order Dispersion and Optical Time Delay

Haiyun Xia, *Student Member, OSA* and Jianping Yao, *Senior Member, IEEE, Member, OSA*

***Abstract*—In the complete reconstruction of ultrashort optical pulses based on temporal interferometry, the chromatic dispersion and the optical time delay are two key factors, which determine the measurement accuracy. Due to the higher order dispersion, the wavelength-to-time mapping becomes nonlinear, leading to a nonuniformly spaced interference pattern and a decreased fringe visibility in the time domain, even though the input pulse is transform limited. On the other hand, an estimation of the time delay difference with a minor deviation from the true value will result in an artificial linear chirp in the reconstructed phase of the pulse under test. In this paper, a rigorous mathematical analysis on the nonlinear frequency-to-time mapping is performed, with which the phenomena of a nonuniformly spaced interference pattern and a decreased fringe visibility are explained. A frequency-to-time mapping function including higher order dispersion is developed. With a general mapping function, using a transform-limited pulse as the reference signal, we propose a method for real-time tracking of the system parameters, including the chromatic dispersion corresponding to all the optical devices incorporated in the system and the time delay introduced by the interferometer. Finally, a complete reconstruction of a 237 fs optical pulse is demonstrated experimentally with an average angular error of 0.18 rad ranging from 190.65 to 193.85 THz.**

***Index Terms*—Chromatic dispersion, phase reconstruction, Sagnac-loop filter, subpicosecond, temporal interferometry.**

I. Introduction

DURING the past two decades, tremendous progress in ultrashort optical pulse generation and its applications in both fundamental and applied studies has created significant demand for fast and accurate characterization of ultrashort optical pulses [1]. Great efforts have been directed toward finding solutions to retrieve the magnitude and phase information of an ultrashort pulse, with the approaches implemented based on spectrographic, tomographic, or interferometric analyses. A simple approach to characterizing an ultrafast pulse is to use optical autocorrelation. The major limitation of the approach is that the pulse shape information is needed, which is usually unknown, making the characterization with low accuracy. In addition, a specific second-order harmonic generation crystal is needed in performing the autocorrelation, which makes the system complicated and costly. Considering that the intensity of an ultrashort pulse is always nonnegative, Peatross and Rundquist proposed an iterative decorrelation algorithm that allows a complete and accurate reconstruction of an optical pulse [2]. Since the iterative algorithm is time consuming, the characterization cannot be implemented in real time. The frequency-resolved optical gating (FROG) [3] and the spectral phase interferometry for direct electric-field reconstruction (SPIDER) [4] are two other important techniques for pulse characterization. FROG is a technique based on spectrographic analysis, in which an ultrashort pulse is characterized based on the information from a spectrally resolved autocorrelation signal followed by an iterative phase-retrieval algorithm. A similar technique, known as time-resolved optical gating (TROG), has also been reported [5]. SPIDER is a technique based on self-referencing spectral interferometry, which allows noniterative, thus fast reconstruction of an optical pulse by generating a spectral shear between two replicas of the pulse to be characterized [6]. Since a frequency-resolving free-space optical grating in FROG/TROG or a frequency-shearing nonlinear material in SPIDER is needed, these techniques are usually implemented in free space, thus suffering from the problems such as phase-matching deviation, spatial beam distortion, and poor focusability. General discussions on techniques for ultrashort optical pulse characterization can be found in [7], [8]. Readers may also refer to [9] for information about the state-of-the-art ultra-pulse characterization systems.

Fortenberry *et al.* proposed a simple approach for complete characterization of short optical pulses based on temporal interferometry (TI) [10], [11]. In the proposed system, an input pulse under test (PUT) was sent to a dispersive element to stretch the PUT until it is long enough to be detected using a high-speed photodetector (PD). The temporally stretched optical pulse was sent to an optical interferometer. The magnitude and phase information of the input pulse was then obtained by analyzing the temporal interferogram at the output of the interferometer. This method is similar to SPIDER in which an ultrashort pulse is characterized based on self-referencing interferometry with a noniterative algorithm, but with the capability of achieving a

Manuscript received February 19, 2009; revised June 25, 2009. First published July 24, 2009; current version published September 17, 2009. This work was supported by the Natural Sciences and Engineering Research Council of Canada (NSERC) through its Strategic Project Grants Program. The work of H. Xia was supported by a scholarship from the China Scholarship Council.

H. Xia is with the Microwave Photonics Research Laboratory, School of Information Technology and Engineering, University of Ottawa, Ottawa ON K1N 6N5, Canada, and also with the Institute of Optoelectronics Engineering, Beijing University of Aeronautics and Astronautics, Beijing 100083, China.

J. Yao is with the Microwave Photonics Research Laboratory, School of Information Technology and Engineering, University of Ottawa, Ottawa ON K1N 6N5, Canada (e-mail: jpyao@site.uottawa.ca).

Color versions of one or more of the figures in this paper are available online at http://ieeexplore.ieee.org.

Digital Object Identifier 10.1109/JLT.2009.2028247

complete characterization of single-shot subpicosecond optical pulses up to a repetition rate of hundreds of megahertz since the interferogram is recorded in the time domain.

TI method has been reported for characterization of ultrashort optical pulses using Fourier or Hilbert transformation algorithms [12], [13]. In these works, as has been pointed out, the frequency-to-time mapping process was assumed to be linear, i.e., the time variable of the temporal interferogram is proportional to the frequency of the spectral interferogram with a fixed ratio given by the integral group velocity dispersion (GVD) of the dispersive elements incorporated in the system. TI method has also been reported to characterize the chromatic dispersion of optical devices [14], [15]. The phase response of a device under test was obtained by a simple and direct subtraction of a reference phase, which is recorded by sending a same short pulse while taking away the device under test.

The primary interest of this paper focuses on the theoretical analysis of the effects of the higher order dispersion on the complete characterization of subpicosecond optical pulses based on TI. An accurate impulse response function associated with the third-order dispersion (TOD) is developed strictly to explain the decrease of the fringe visibility observed in the temporal interferogram. We point out that the higher order dispersion has been underestimated in the previous literature. The temporal interferogram becomes nonuniform obviously when the pulsewidth is narrow than one picosecond, even the pulse is transform limited. In such a case, a nonlinear frequency-to-time mapping function that considers higher order dispersion is deduced theoretically to explain these phenomena. Thanks to the advantage of the TI method, the PUT and the transform-limited optical pulse used as a reference can be recorded in one repetition interval of the pulsed laser source. With the real-time tracking of the system parameters, a complete characterization of the PUT is performed accurately, although the system may suffer from the environmental changes.

We would like to emphasize that the key difference of the technique in this paper is that all order dispersion in the entire system is considered in the time-to-frequency transform, while in the previous work [12], only the GVD of the dispersive element, such as a dispersion compensating fiber (DCF), is considered. In fact, the PUT experiences pulse stretching and compression in the entire system depending on the sign of the dispersion of each optical element. An insufficient estimation of the chromatic dispersion associated with the entire system will introduce errors to the reconstructed magnitude and phase of the PUT.

The remainder of the paper is organized as follows. In Section II, we start with the nonlinear Schrodinger equation (NLSE) to evaluate the maximum power that can be used to avoid nonlinear effects in the characterization system. Then, a theoretical analysis is provided to describe the nonlinear frequency-to-time mapping, with which the phenomena of nonuniformly spaced interference pattern and a decreased fringe visibility are explained. In Section III, an experiment to characterize subpicosecond optical pulses based on the developed nonlinear frequency-to-time mapping is performed. A discussion on the stability and sensitivity of the proposed technique is presented in Section IV. Finally, a conclusion is drawn in Section V.

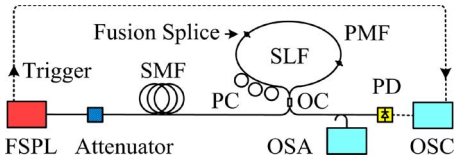

Fig. 1. Schematic diagram of the system for ultrashort optical pulse characterization. FSPL: femtosecond pulse laser; SMF: single-mode fiber; PC: polarization controller; OC: optical coupler; SLF: Sagnac-loop filter; PMF: polarization maintaining fiber; PD: photodetector; OSC: oscilloscope; OSA: optical spectrum analyzer.

II. Principle

The schematic diagram of the system used for our analysis and experiment is shown in Fig. 1. The system consists of a femtosecond pulsed laser (FSPL) source, a dispersive element, a Sagnac-loop filter (SLF), and a PD. A tunable optical attenuator is incorporated after the FSPL to eliminate the nonlinearity in the system. The dispersive element is a length of standard single-mode fiber (SSMF). When a subpicosecond pulse is transmitting through the SSMF, the pulse will be stretched in time due to the chromatic dispersion of the fiber. Then, the stretched pulse is sent to the SLF, which consists of a 3-dB optical coupler, a polarization controller (PC), and a polarization maintaining fiber (PMF). Two duplicated pulses with a time delay difference introduced by the PMF are obtained at the output of the SLF. The polarization state of the light wave at one end of the PMF is rotated by the PC to make the temporal interferogram have the largest visibility. The temporal and spectral interferograms are recorded using an oscilloscope (OSC) and an optical spectrum analyzer (OSA), respectively.

To eliminate the nonlinear effects, the peak power of the input pulse should be controlled at a low level. Then, the SSMF can be considered as a linear component. To quantitatively evaluate the maximum power that can be used to make the nonlinearity negligible in the system, we start our analysis from the NLSE. A normalized NLSE is given as [16]

$$i\frac{\partial U}{\partial \xi}=\frac{\operatorname{sgn}(\beta_2)}{2}\frac{\partial^2 U}{\partial \tau^2}+\frac{i\beta_3}{6|\beta_2|T_0}\frac{\partial^3 U}{\partial \tau^3}-N^2|U|^2U\exp(-\alpha\xi L_d) \tag{1}$$

where $\xi = z/L_d$ and $\tau = (t - z/v_g)/T_0$ are two normalized variables representing the propagation location along the SSMF and the retarded time, respectively, T_0 is the half-width at $1/e$ intensity point of the input pulse, v_g is the group velocity, $U(\xi, \tau)$ is the normalized amplitude such that the amplitude of pulse envelope is $P_0^{1/2}\exp(-\alpha\xi L_d/2)U$, and P_0 is the peak power of the input pulse. The GVD length $L_d = T_0^2/|\beta_2|$, the TOD length $L'_d = T_0^3/|\beta_3|$, and the nonlinear length $L_{\mathrm{NL}} = 1/\gamma P_0$ provide the length scale over which the dispersion and the nonlinear effects become important, where $\gamma = n_2\omega_0/cA_{\mathrm{eff}}$ is the nonlinear coefficient, n_2 is the nonlinear index, ω_0 is the carrier frequency, and A_{eff} is the effective core area. The ratio of L_d to L_{NL} gives the nonlinear factor $N^2 = \gamma P_0 T_0^2/|\beta_2|$. The nonlinear fact N should be small enough to avoid the nonlinear effects. For example, for SSMF, we have $\beta_2 \approx -22\ \mathrm{ps}^2/\mathrm{km}$, $\beta_3 \approx 0.13\ \mathrm{ps}^3/\mathrm{km}$, and $\gamma \approx 1.2\ \mathrm{W}^{-1}\mathrm{km}^{-1}$. Given $T_0 \approx 200$ fs, then $L_d \approx 1.8$ m and $L'_d \approx 80$ m. If $N < 0.01$, then the peak power should be lower than 46 mW.

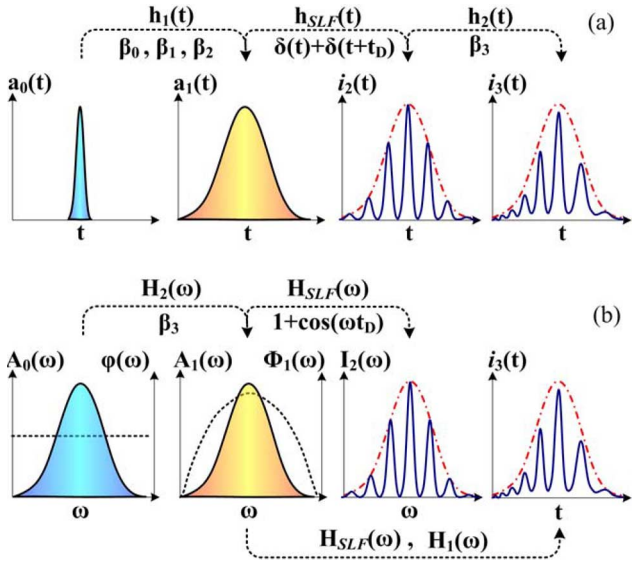

Fig. 2. Investigation of the effects of higher order dispersion on the complete reconstruction of ultrashort optical pulses based on TI. (a) The system is modeled as a cascade of three subsystems having impulse responses of $h_1(t)$, $h_{\rm SLF}(t)$, and $h_2(t)$ in the time domain. (b) The system is modeled as a cascade of three subsystems having transfer functions of $H_2(\omega)$, $H_{\rm SLF}(\omega)$, and $H_1(\omega)$ in the frequency domain.

In addition, considering the GVD length L_d and the TOD length L'_d are comparable, we think the TOD is not negligible. In the following discussion, we will perform an analysis considering the higher order dispersion.

Under the low-power assumption, the entire system is linear. For this reason, the effects associated with different orders of dispersion can be regarded as contributions from many cascaded subsystems, and the entire system transfer function is the multiplication of the transfer functions associated with all these subsystems. In addition, the system transfer function is independent of the orders of cascade due to the property of linear system. For convenience, the orders of the subsystems are changed in the following analyses.

The transfer function of an SSMF can be expressed by expanding the mode-propagation constant β in a Taylor series [16]

$$H(\omega) = H_0 \exp\left(-j\sum_{n=0}^{\infty}\frac{\beta_n L}{n!}\omega^n\right) \tag{2}$$

where β_n is the nth order mode-propagation constant, H_0 is a constant which is unity if the loss of the fiber is ignored, ω is the angular frequency measured relative to the center frequency of the pulse, and L is the length of the SSMF.

We first analyze a system consisting of three cascaded subsystems, as shown in Fig. 2(a). The first subsystem associated with the dispersion up to the GVD has a transfer function given by

$$H_1(\omega) = H_0 \exp\left(-j\sum_{n=0}^{2}\frac{\beta_n L}{n!}\omega^n\right). \tag{3}$$

The impulse response $h_1(t)$ is the inverse Fourier transform of $H_1(\omega)$, which can be expressed as

$$h_1(t_R) = h_0 \exp\left(jt_R^2/2\beta_2 L\right) \tag{4}$$

where $t_R = t - \beta_1 L$ is the time measured relative to the average time delay and $h_0 = H_0(j2\pi\beta_2 L)^{-1/2}\exp(-j\beta_0 L)$ is the complex amplitude. The complex envelope $a_1(t)$ under the effect of the chromatic dispersion up to the GVD can be expressed as a convolution between the input ultrashort pulse $a_0(t)$ and $h_1(t)$

$$\begin{aligned} a_1(t) &= \int_{-\infty}^{\infty} a_0(t')h_1\left(t_R - t'\right)dt' \\ &= h_0\int_{-\infty}^{\infty} a_0(t')\exp\left[j(t_R - t')^2/2\beta_2 L\right]dt' \\ &= h_0\exp\left(jt_R^2/2\beta_2 L\right) \\ &\quad\times\int_{-\infty}^{\infty} a_0(t')\exp(jt'^2/2\beta_2 L) \\ &\qquad\times\exp(-jt't_R/2\beta_2 L)dt'. \end{aligned} \tag{5}$$

If the pulsewidth meet the condition that $|T_0^2/\beta_2 L| \ll 1$ i.e., $L_d \ll L$, then (5) can be well approximated by

$$\begin{aligned} a_1(t) &= h_0\exp\left(jt_R^2/2\beta_2 L\right)\int_{-\infty}^{\infty} a_0(t')\exp(-jt't_R/2\beta_2 L)dt' \\ &= h_0\exp\left(jt_R^2/2\beta_2 L\right)\left[A_0(\omega)\right]_{\omega=t_R/\beta_2 L} \end{aligned} \tag{6}$$

where $A_0(\omega)$ is the Fourier transformation of $a_0(t)$, with an angular frequency given by $\omega = t_R/\beta_2 L$. Hence, under the conditions of $L_d \ll L$ and low peak power, considering the dispersion up to the GVD, the output pulse in the time domain is analogous to its original spectrum with a scaling factor of $\ddot{\Phi} = \beta_2 L$ [17]. This real-time optical spectrum analysis has also been proposed by using a chirped fiber grating [18]. When a linearly chirped fiber Bragg grating is used, the dispersion ripples deviating from a designed chirp rate will be a deleterious factor in the reconstruction of an ultrashort pulse.

The second subsystem associated with a two-tap SLF has an impulse response function of

$$h_{\rm SLF}(t) = \left[\delta(t) + \delta(t + t_D)\right]/2 \tag{7}$$

where $\delta(t)$ is the Dirac delta function, and t_D is the time delay difference between the two time-delayed replicas. The electrical field of the signal at the output of the SLF is given by

$$a_2(t) = a_1(t) * h_{\rm SLF}(t) \tag{8}$$

where $*$ denotes the convolution operation. The electric current of the PD can be written as

$$\begin{aligned} i_2(t) &= \Re a_2(t)\cdot\overline{a_2(t)} \\ &= \frac{\Re|h_0|^2}{4}\Big\{|A_0(\omega)|^2 + |A_0(\omega+\Delta\omega)|^2 \\ &\qquad + 2\,|A_0(\omega)|\,|A_0(\omega+\Delta\omega)| \\ &\qquad\times\cos\left[\omega t_D + \Delta\varphi(\omega)\right]\Big\}_{\omega=t_R/\beta_2 L} \end{aligned} \tag{9}$$

where $\Re$ is the responsivity of the PD, $\overline{a_2(t)}$ is a complex conjugate of $a_2(t)$, $\Delta\omega = t_D/\beta_2 L$ is the corresponding frequency shear due to the time delay difference, $\Delta\varphi(\omega) = \varphi(\omega) - \varphi(\omega + \Delta\omega)$ is the relative phase between a pair of successive frequency

components separated by $\Delta\omega$. If $\Delta\omega$ is small enough, (9) can be written as

$$i_2(t) = \frac{1}{2}\Re|h_0|^2 I_0(\omega)\left\{1+\cos\left[\omega t_D + \Delta\varphi(\omega)\right]\right\}_{\omega=t_R/\beta_2 L} \tag{10}$$

where $I_0(\omega) = |A_0(\omega)|^2$ is the spectral intensity of the original pulse. From (10), one can see that the temporal interferogram carries the information of both the spectral intensity and the relative phase. If $\Delta\varphi(\omega)$ is a constant, then the temporal interferogram would have a constant period of $T_c = 2\pi\beta_2 L/t_D$.

The third subsystem associated with the TOD has a transfer function expressed by

$$H_2(\omega) = \exp\left(-j\frac{\beta_3 L}{6}\omega^3\right). \tag{11}$$

The impulse response $h_2(t)$ corresponding to $H_2(\omega)$ has been expressed using the Airy function [19]. However, we perform an inverse Fourier transform to $H_2(\omega)$ directly by using the integral table [20]. A close-form expression of $h_2(t)$ is then given by

$$\begin{aligned} h_2(t) &= \frac{1}{2\pi}\int_{-\infty}^{\infty} H_2(\omega)\exp(j\omega t)d\omega \\ &= \frac{1}{\pi}\int_0^{\infty}\cos\left(\omega t - \frac{\beta_3 L}{6}\omega^3\right)d\omega \\ &= \begin{cases} \frac{1}{3}\sqrt{\frac{2t}{\beta_3 L}}\left[J_{\frac{1}{3}}\left(\frac{2}{3}\sqrt{\frac{2t^3}{\beta_3 L}}\right)\right. \\ \quad \left. + J_{-\frac{1}{3}}\left(\frac{2}{3}\sqrt{\frac{2t^3}{\beta_3 L}}\right)\right] & \text{when } t>0 \text{ and } \beta_3>0 \\ \frac{1}{3\pi}\sqrt{\frac{-6t}{\beta_3 L}}K_{\frac{1}{3}}\left(\frac{2}{3}\sqrt{\frac{-2t^3}{\beta_3 L}}\right) & \text{when } t<0 \text{ and } \beta_3>0 \end{cases}. \end{aligned} \tag{12}$$

In deducing (12), the following two integrals are used.

$$\begin{aligned} &\int_0^{\infty}\cos(a^3x^3)\cos(bx)dx \\ &= \frac{\pi}{6a}\sqrt{\frac{b}{3a}}\left[J_{\frac{1}{3}}\left(\frac{2b}{3a}\sqrt{\frac{b}{3a}}\right) + J_{-\frac{1}{3}}\left(\frac{2}{3}\sqrt{\frac{b}{3a}}\right)\right. \\ &\qquad \left. + \frac{\sqrt{3}}{\pi}K_{\frac{1}{3}}\left(\frac{2b}{3a}\sqrt{\frac{b}{3a}}\right)\right] \quad (a>0, b>0) \end{aligned} \tag{13a}$$

$$\begin{aligned} &\int_0^{\infty}\sin(a^3x^3)\sin(bx)dx \\ &= \frac{\pi}{6a}\sqrt{\frac{b}{3a}}\left[J_{\frac{1}{3}}\left(\frac{2b}{3a}\sqrt{\frac{b}{3a}}\right) + J_{-\frac{1}{3}}\left(\frac{2}{3}\sqrt{\frac{b}{3a}}\right)\right. \\ &\qquad \left. - \frac{\sqrt{3}}{\pi}K_{\frac{1}{3}}\left(\frac{2b}{3a}\sqrt{\frac{b}{3a}}\right)\right] \quad (a>0, b>0) \end{aligned} \tag{13b}$$

where $J_m(z)$ and $K_m(z)$ are the mth-order Bessel function of the first kind and the mth-order modified Bessel function of the second kind, respectively.

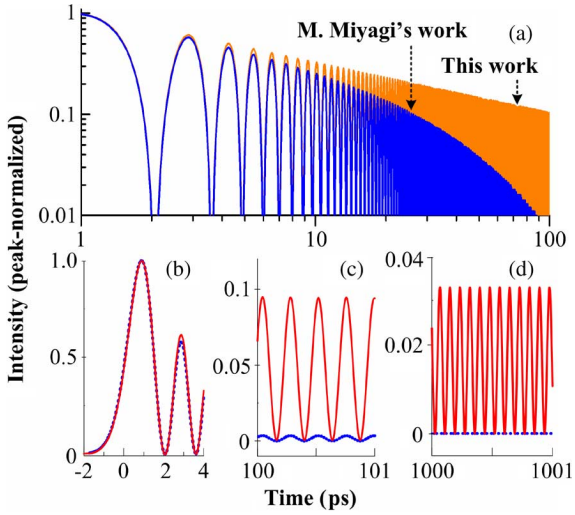

Fig. 3. (a) Impulse response associated with the TOD shown on a logarithmic scale and (b), (c), (d) partial views of the impulse response shown on a linear scale.

With the parameters $\beta_3 = 0.13\ \text{ps}^3/\text{km}$ and $L \approx 10.6\ \text{km}$ used in this paper, $|h_2(t)|^2$ is calculated and compared with Miyagi and Nishida's work [19], as shown in Fig. 3. As can be seen in Fig. 3(a), although the impulse responses associated with the TOD for the two methods show good agreement in a small time range from 1 to 100 ps, it is obvious that the damping speed of the oscillations corresponding to (12) is much slower than that of the impulse response function described in [19]. As shown in Fig. 3(d), the long tail on the trailing side can even extend to one nanosecond away with a normalized intensity of 0.035. This time scale is usually comparable to the period T_c. Considering the effect of the TOD, the final temporal interferogram $i_3(t)$ is the convolution between $i_2(t)$ and $|h_2(t)|^2$. Thus, the fringe visibility of the temporal interferogram will decrease obviously, as shown in Fig. 2(a). It is observed that the smaller the T_c, the lower the fringe visibility of the temporal interferogram, which will be shown in Figs. 5 and 6.

Since the impulse response associated with the TOD is asymmetric, one can imagine that the period of the temporal interferogram will be modulated according to the property of the convolution. To study the period change in the temporal interferogram, we consider that the entire system consists of three cascaded subsystems having transfer functions of $H_2(\omega)$, $H_{\text{SLF}}(\omega)$, and $H_1(\omega)$, as shown in Fig. 2(b).

In the frequency domain, the interferogram recorded by an OSA is the product of the pulse spectrum and the transfer function of the SLF

$$I_2(\omega) = I_0(\omega)\left[1+\cos(\omega t_D)\right]. \tag{14}$$

This spectral interferogram carries no phase information of the PUT.

On the other hand, the complex spectrum of the original pulse can be written as $A_0(\omega)\exp[j\varphi(\omega)]$. Then, under the effects of TOD, the complex spectrum is

$$\begin{aligned} A_1(\omega) &= A_0(\omega)\exp\left[j\varphi(\omega)\right]H_2(\omega) \\ &= A_0(\omega)\exp\left\{j\left[\varphi(\omega) - \Phi_1(\omega)\right]\right\} \end{aligned} \tag{15}$$

where $\Phi_1(\omega) = \beta_3 L\omega^3/6$. The chromatic dispersion up to GVD performs an optical Fourier transform as described by (6). So, considering the dispersion up to the TOD, using (6) and (15), the complex spectrum can be expressed as

$$a_1'(t) = h_0 \exp\left(jt_R^2/2\beta_2 L\right)\left[A_1(\omega)\right]_{\omega=t_R/\beta_2 L}. \tag{16}$$

Using the same process as having been described from (6) to (9), the final temporal interferogram can be expressed as

$$i_3(t) = \frac{1}{2}\Re|h_0|^2 I_0(\omega) \times \left\{1+\cos\left[\omega t_D + \Delta\varphi(\omega) - \Delta\Phi_1(\omega)\right]\right\}_{\omega=t_R/\beta_2 L}. \tag{17}$$

For simplicity, we assume that the original pulse is nearly transform limited, i.e., $\Delta\varphi(\omega) \approx 0$. Then, the phase of the cosine term in (17) is

$$\begin{aligned}\Phi &= \left[\omega t_D - \Delta\Phi_1(\omega)\right]_{\omega=t_R/\beta_2 L} \\ &= \left[\omega t_D - \frac{\partial\Phi_1(\omega)}{\partial\omega}\Delta\omega\right]_{\omega=t_R/\beta_2 L} \\ &= \frac{t_R}{\beta_2 L}t_D - \frac{\beta_3 L}{2}\left(\frac{t_R}{\beta_2 L}\right)^2\frac{t_D}{\beta_2 L} \\ &= \omega' t_D\end{aligned} \tag{18}$$

where the angular frequency is $\omega' = (t_R/\beta_2 L) - (\beta_3 L t_R^2/2(\beta_2 L)^3)$. So, consider the TOD, the temporal interferogram (17) is still analogous to the spectral interferogram. But the time-to-frequency transform becomes nonlinear. For example, for SSMF, we have $D \approx 17$ ps/km/nm, given the spectral width of the origin pulse is 10 nm, then ω' changes 2.28% within the full-width at half-maximum (FWHM). So, in a precise reconstruction of optical pulses that have a duration narrower than one picosecond, the effect of the TOD is not negligible.

Using the same process from (15) to (18), higher order dispersion can be considered, which yields a general form of the angular frequency as a polynomial function of t_R

$$\omega' = \frac{t_R}{\beta_2 L} - \sum_{n=3}^{\infty}\frac{\beta_n L t_R^{n-1}}{(n-1)!(\beta_2 L)^n}. \tag{19}$$

With the assumption of a transform-limited input pulse, the current detected by the PD can be expressed as

$$i_3(t) = \frac{1}{2}\Re|h_0|^2 I_0(\omega)\left[1+\cos(\omega' t_D)\right]. \tag{20}$$

From (14) and (20), one can see that, with an angular frequency given by (19), the temporal interferogram is still analogous to the spectral interferogram even under the effect of the higher order dispersion. Thus, one can record the spectral interferogram and the temporal interferogram simultaneously and perform a polynomial fitting of the corresponding points on the two interferograms to realize a complete tracking of the chromatic dispersion associated with the entire system.

III. Experiment

A femtosecond pulse generated by a passively mode-locked fiber laser (IMRA Femtolite 780 Model B-4-FC-PD) is used in the experiment. To avoid nonlinear effects, first, we measure the pulsewidth to evaluate the maximum input power. The intensity profile is measured using an optical autocorrelator (Femtochrome Model FR-103MN). The fiber laser and the optical autocorrelator are connected using a fiber jumper with a length of only 16 cm; so, the pulse stretching due to the fiber jumper is negligible. The output from the autocorrelator is shown in Fig. 4. The conversion of the FWHM of the autocorrelation trace ΔT to the FWHM of the pulse Δt is dependent on the pulse shape. With a Gaussian shape assumption, we have $\Delta t = \sqrt{2}k\Delta T/2$, where $k = 7.5$ ps/ms is a calibration factor. Then, the FWHM of the laser pulse is calculated to be 394 fs ($T_0 = 237$ fs). So the peak power should be lower than 33 mW according to the analysis in Section II. When the input power is above this value, the temporal interferogram and spectral interferogram are measured, as shown in Fig. 5. It is obvious that the profile varies from the Gaussian shape into the hyperbolic secant shape, which indicates that a nonlinear effect is resulted due to the self-phase modulation [16]. Comparing the two interferograms in Fig. 5, one can see a decrease in fringe visibility in the time domain, which has been predicted in the earlier analysis. The ripple in the spectral interferogram is due to the power fluctuations during the scanning process of the OSA, which takes about 30 s.

To perform a complete characterization of an optical pulse, the sampling interval should be narrow than the Nyquist limit. According to the Whittaker–Shannon sampling theorem, since the temporal interferogram has a period about T_c, the sampling frequency f_s should satisfy the condition $f_s > 2/T_c$, i.e., a sampling of the spectrum at a frequency higher than $t_D/\pi\beta_2 L$ would be sufficient to reconstruct the amplitude and phase of the pulse. According to (10), the spectral phase $\varphi(\omega)$ is obtained

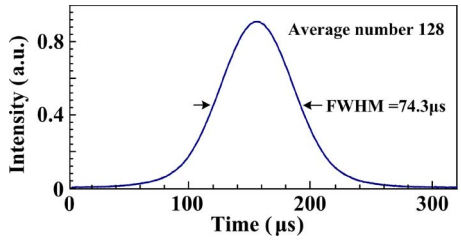

Fig. 4. Optical autocorrelation of the femtosecond laser pulse.

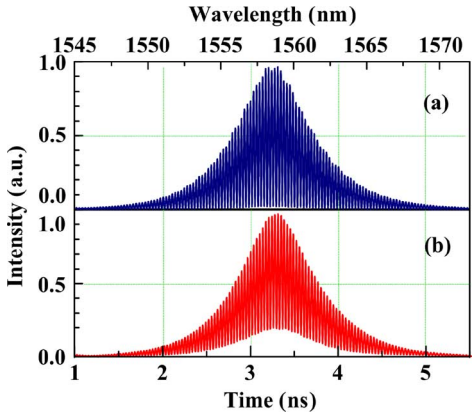

Fig. 5. Interferograms (a) spectrum interference pattern record on the OSA; (b) temporal interference pattern recorded on the OSC. $t_D = 38.67$ ps is used.

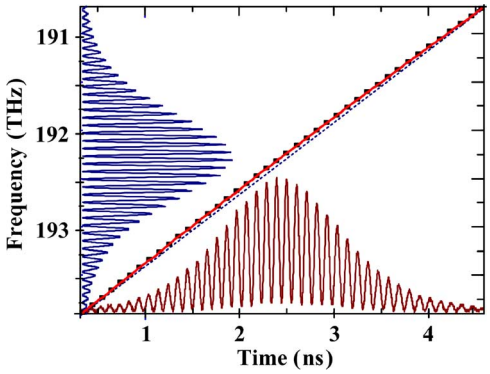

Fig. 6. Calibrated time-to-frequency mapping function. A fourth-order polynomial fitting of the corresponding peaks in the time domain and the frequency domain. $t_D = 12.54$ ps is used. Under the effect of higher order dispersion, the derived time-to-frequency conversion function (solid line) deviates from a straight line (dot line) slightly.

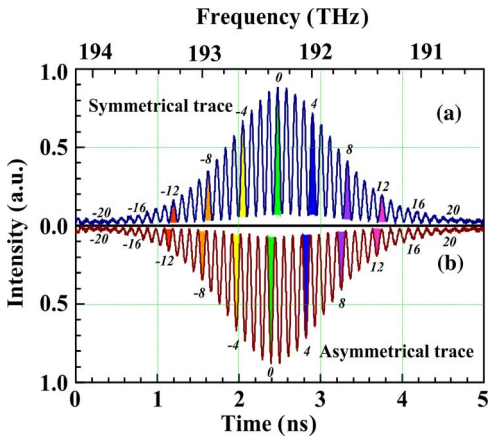

Fig. 7. (a) spectral interferogram transformed from the time domain to the frequency domain and (b) the temporal interferogram recorded on the OSC. The order of interference is numbered relative to the center peak.

by integrating $\Delta\varphi(\omega)$ over all the successive frequency components separated by $\Delta\omega$ within the whole spectrum. An experiential evaluation of the spectral shear is $\Delta\omega \approx 3\%W_0$, where W_0 is the spectral FWHM of the PUT. On the other hand, the time delay difference t_D should be large enough relative to the pulsewidth T_0 to perform the Fourier-transform algorithm, as will be shown in Fig. 8(a). Finally, for a given bandwidth of the receiver, the second-order dispersion $\beta_2 L$ can be chosen to optimize the sensitivity of the system.

To carry out a complete reconstruction of a subpicosecond pulse, we need to consider the effect of higher order dispersion. To achieve this purpose, a polynomial frequency-to-time mapping function is used according to (19). In the following experiment, the PD and the OSC both have a bandwidth of 50 GHz. The pulse directly generated from the FSPL is nearly transform limited, which allows a complete calibration of the higher order dispersion in the entire system. The temporal interferogram obtained from the OSC and the spectrum interferogram obtained from the OSA are shown along the abscissa and the ordinate in Fig. 6, respectively. The peak centers of the two patterns are found using a single-peak fitting algorithm. A polynomial fitting function considering higher order dispersion up to the fourth order, which relates the corresponding peak centers of the two patterns, is obtained [14]

$$f = a_0 + a_1 t + a_2 t^2 + a_3 t^3 + a_4 t^4 \tag{21}$$

where $a_0 = 1.942 \times 10^{14}$, $a_1 = -7.934 \times 10^{20}$, $a_2 = 7.519 \times 10^{27}$, $a_3 = 9.377 \times 10^{35}$, and $a_4 = -1.105 \times 10^{44}$ are the fitting parameters. One can retrieve the fiber parameters by drawing a comparison between (19) and (21). For example, $a_1 = 1/2\pi\beta_2 L$, if the fiber length is known, the GVD parameter β_2 can be calculated.

Instead of using only the GVD coefficient, (21) is used to build the relation between the temporal interferogram and the spectral interferogram in this paper. First, we use this nonlinear mapping function to reconstruct the pulse generated from the FSPL. Since the pulse has also been measured using an optical autocorrelator, we can demonstrate the accuracy of the reconstruction and see whether the original pulse is transform limited or not. The nonlinear mapping function (21) incorporates higher order dispersion associated with all optical components in the system. In addition, with (21), we can perform a real detection of the time delay difference t_D, which will be discussed later in this section.

The temporal interferogram recorded on the OSC is transformed into the frequency domain using (21), as shown in Fig. 7. For an easy comparison, the temporal interferogram is flipped vertically in Fig. 7(b). Due to the higher order dispersion, one can see the nonperiodic change in the time domain.

We employ the phase-retrieval algorithm [21] to reconstruct the intensity and phase of the input ultrashort pulse. As the first step, the spectral interferogram in Fig. 7(a) is inverse Fourier transformed. The result is shown in Fig. 8(a). Then, the right sideband in Fig. 8(a) is selected, which represents the interference term in (9). The selected sideband is shifted by t_D to the origin, then Fourier transformed to retrieve the spectral intensity and to calculate the spectral phase by integrating the relative phase at discrete frequencies, as shown in Fig. 8(b). As the final step, the temporal intensity and phase of the original pulse is obtained by calculating the inverse Fourier transform of the spectrum in Fig. 8(b), with the result shown in Fig. 8(c). It has been pointed out that the original pulses and the stretched pulses have the same spectrum; thus, if the temporal resolution of an OSC is not high enough to characterize the original pulses, it would not be able to characterize the stretched pulses either [12]. However, in this paper, the required sampling rate is determined by the frequency of the temporal interferogram. In the inverse Fourier transform as the last step, by adding zero values at both sides of the spectrum in Fig. 8(b), we can improve the sampling rate in the time domain. The reconstructed intensity profile in the time domain is compared with the Gaussian intensity profile measured using an optical autocorrelator, an excellent agreement is reached. The product of the temporal and spectral widths (both measured as FWHM) is 0.433, which indicates that the original pulse is nearly transform limited. To show the impact of the higher order dispersion on the proposed technique, we reconstruct the phase and the intensity profiles of the ultrashort pulse using a linear fitting in the calibration procedure, i.e., only the GVD is considered. The result is shown in

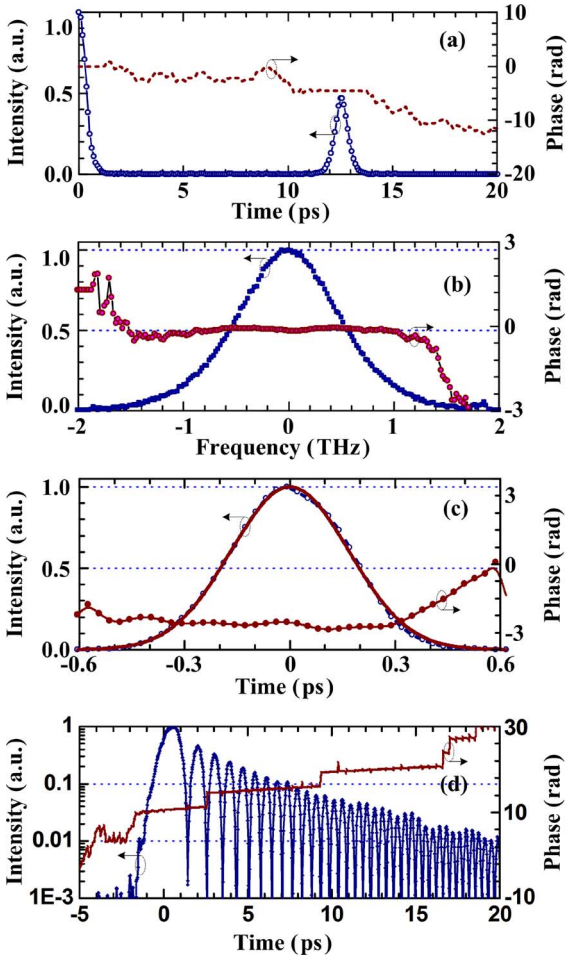

Fig. 8. (a) Intensity and phase of the inverse Fourier transform of the spectral interferometric pattern. (b) Reconstructed spectral intensity and phase relative to the frequency center of the input pulse at 192.31 THz. (c) Reconstructed temporal intensity and phase of the input pulse. The reconstructed intensity profile is compared with the estimated Gaussian profile based on optical autocorrelation (solid curve). (d) Reconstructed temporal intensity and phase profiles of the input pulse using a linear frequency-to-time conversion. The reconstructed pulse is significantly broadened.

Fig. 8(d). As can be seen, the pulse is broadened. The broadening is mainly due to the TOD, which has been predicted by (12). Some jumps in the phase profile corresponding to the zero intensity points are also observed. Obviously, without considering the effect of the higher order dispersion, the reconstructed intensity profile of the PUT is significantly broadened with a large characterization error. It is therefore important to take the high-order dispersion into consideration in the reconstruction of an ultrashort pulse.

To show the significance of the real-time tracking technique proposed in this paper, we incorporate a 10.9 m SSMF into the system by using two optical couplers, as shown in Fig. 9. As pointed out earlier, during the reconstruction process an error estimation of the time delay difference t_D will result in an artificial linear frequency chirp in the reconstructed phase of the PUT. This problem can be solved by using an interferometer with a feedback loop to minimize the time delay error [13]. However, for an optical source has a megahertz repetition rate, the feedback loop can only improve the long-term stability. In this work,

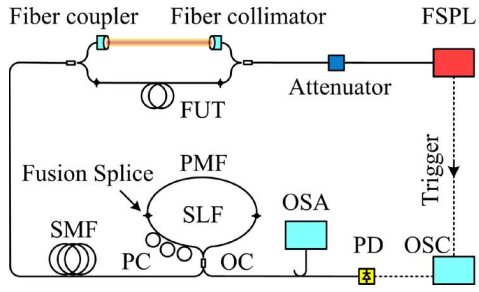

Fig. 9. Schematic diagram of the proposed apparatus with a function of real-time calibration. FUT: fiber under test.

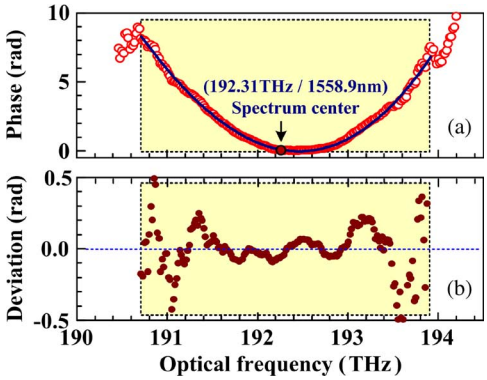

Fig. 10. (a) Measured phase response of a 10.9 m long SSMF (circles) and the calculated phase response (solid line) using dispersion parameters up to the third-order derived from the frequency dependence of the group delay; (b) The phase errors between the two measured methods.

the FSPL has a repetition rate of 48.6 MHz and the pulses are stretched to have a FWHM of 1.5 ns, as shown in Fig. 7(b). Thus, we can record the transform-limited pulse and the PUT within one repetition interval of the FSPL. A tunable delay line composed of a pair of pigtailed fiber collimator and coupler is used to avoid temporal overlap of the two object pulses. According to (14), with a spectral interferogram obtained via a nonlinear time-to-frequency transform from the time domain to the frequency domain, as shown in Fig. 7(a), a real-time measurement of t_D is performed. The time delay difference is estimated to have a value of 12.54 ps from Fig. 7(a). Then, the phase of the pulse going through the additional fiber is retrieved and compared with the phase calculated using the dispersion parameters obtained based on the modulation phase shift method [22]. An excellent agreement is achieved, as shown in Fig. 10(a). Due to the higher order dispersion of the fiber, the phase response is not symmetrical about the carrier frequency of the optical pulse. The average error between the two measurements is 0.18 rad for a spectral range from 190.65 to 193.85 THz, as shown in Fig. 10(b).

IV. Discussions

In this work, a long SSMF is used as a dispersive element, which makes the system sensitive to the environmental changes. To improve the system stability, a dispersive element with a higher dispersion, such as a DCF or a linearly chirped fiber Bragg grating, can be used. Since the length of a DCF or a

linearly chirped fiber Bragg grating is much shorter, the stability would be significantly improved. The drift of the PC in the SLF due to thermal or other environmental changes is another factor that will affect the long-term stability of the system. Although the all-fiber SLF can be well packaged to minimize the impact from the environmental disturbance, the time delay difference may vary slowly due to the drift of the PC and the strain and temperature-induced change in the PMF; thus, the real-time tracking of the time delay difference in the proposed approach is still important.

To characterize pulses in a high-repetition-rate pulse train, the pulses after the frequency-to-time mapping should not overlap; therefore, the system must have a finite dispersion. For a given dispersion, the sensitivity of the proposed technique is determined by the SNR at the output of the PD. Since the system is implemented using pure fiber-optic components, the system loss is significantly reduced compared with a system based on free-space optics. In addition, the use of a DCF as the dispersive element would further improve the sensitivity since a shorter DCF is needed for a given dispersion, which has a lower attenuation. In addition, the optical signal can be amplified by Raman amplification in the DCF, which has been demonstrated in [23]. We would like to point out that a low-power optical signal could also be amplified before feeding to a pulse characterization system based on FROG, SPIDER, or TROG techniques. However, the phase response of the optical amplifier is added to the PUT and it would be difficult to be subtracted from the reconstructed phase. Furthermore, the pulse characterization techniques, such as FROG, SPIDER, and TROG, are implemented based on nonlinear optics, while the proposed technique is based on linear optics [24]. Thus, for linear optics-based approach, a much lower power is needed to perform a complete pulse reconstruction, which means a higher sensitivity can be achieved using the TI technique.

A direct comparison among different techniques is usually difficult, since the performance of a particular setup is determined by the parameters of the specific system. However, to show the advantage of the TI technique, the sensitivity is evaluated here. For example, a rough evaluation of the sensitivity of a FROG-based system for a single-shot, 800 nm, 100 fs pulse from a regeneratively amplified or unamplified Ti: sapphire oscillator is about 0.01–1 μJ [4]. In this work, for the characterization of a single-shot pulse from a passively mode-locked fiber laser at a center wavelength of 1559 nm and a pulsewidth of $T_0 = 100$ fs, if $N < 0.01$, the peak power P_0 should be lower than 183 mW; then, the pulse energy $E_0 = \sqrt{\pi} P_0 T_0$ is calculated to be 32.4 fJ, which is far below the energy required to achieve the nonlinear interaction used in the FROG technique.

Finally, the polarization state of the pulses often encountered in an optical telecommunication system is usually unknown because of the propagation-induced polarization rotation in optical fibers [8]. Thus, most of the characterization systems based on nonlinear optics should be complemented by polarization diversity [25]. In the proposed technique, however, the intensity and phase of the reconstructed ultrashort pulse are independent of the polarization state of the PUT if the SLF works with two of the channels at the orthogonal polarization states [26].

V. Conclusion

The effect of higher order dispersion on the reconstruction of subpicosecond optical pulses based on TI was investigated theoretically and experimentally. With the mathematical analyses, the decrease in fringe visibility and the change in period in the temporal interferogram due to the higher order dispersion were explained. Instead of using a closed-loop control to improve the stability of the optical interferometer, we proposed to use a transform-limited pulse to perform a real-time tracking of the system parameters, which allows a more precise reconstruction of the PUT, especially for an ultrashort pulse train with high repetition rate and low power. The entire characterization process can be realized by a system to perform real-time data acquisition and processing, which has high potential for practical implementations.

References

[1] G. Steinmeyer, D. H. Sutter, L. Gallmann, N. Matuschek, and U. Keller, "Frontiers in ultrashort pulse generation: Pushing the limits in linear and nonlinear optics," *Science*, vol. 286, no. 10, pp. 1507–1512, 1999.

[2] J. Peatross and A. Rundquist, "Temporal decorrelation of short laser pulses," *J. Opt. Soc. Am. B*, vol. 15, no. 1, pp. 216–222, 1998.

[3] R. Trebino, K. W. DeLong, D. N. Fittinghoff, J. Sweetser, M. A. Krumbügel, and B. Richman, "Measuring ultrashort laser pulses in the time-frequency domain using frequency-resolved optical gating," *Rev. Sci. Instrum.*, vol. 68, no. 9, pp. 3277–3295, 1997.

[4] C. Iaconis and I. A. Walmsley, "Spectral phase interferometry for direct electric-field reconstruction of ultrashort optical pulses," *Opt. Lett.*, vol. 23, no. 10, pp. 792–794, 1998.

[5] R. G. M. P. Koumans and A. Yariv, "Pulse characterization at 1.5 μm using time-resolved optical gating based on dispersive propagation," *IEEE Photon. Technol. Lett.*, vol. 12, no. 6, pp. 666–668, Jun. 2000.

[6] W. Kornelis, J. Biegert, J. W. G. Tisch, M. Nisoli, G. Sansone, C. Vozzi, S. De Silvestri, and U. Keller, "Single-shot kilohertz characterization of ultrashort pulses by spectral phase interferometry for direct electric-field reconstruction," *Opt. Lett.*, vol. 28, no. 4, pp. 281–283, 2003.

[7] I. A. Walmsley and V. Wong, "Characterization of the electric field of ultrashort optical pulses," *J. Opt. Soc. Am. B*, vol. 13, no. 11, pp. 2453–2463, 1996.

[8] C. Dorrer, "High-speed measurements for optical telecommunication systems," *IEEE J. Sel. Topics Quantum Electron.*, vol. 12, no. 4, pp. 843–858, Jul. 2006.

[9] N. Savage, "Ultrashort pulse characterization," *Nat. Photon.*, vol. 3, no. 4, pp. 230–232, 2009.

[10] R. M. Fortenberry, W. V. Sorin, H. Lin, S. A. Newton, J. K. Andersen, and M. N. Islam, "Low-power ultrashort optical pulse characterization using linear dispersion," in *Proc. Opt. Fiber Commun. Conf.*, vol. 6 of 1997 OSA Tech. Digest Series (Opt. Soc. Am., 1997), , pp. 290–291, paper ThL3.

[11] R. M. Fortenberry and W. V. Sorin, "Apparatus for characterizing short optical pulses," U.S. Patent 5,684,586, Nov. 4, 1997.

[12] N. K. Berger, B. Levit, V. Smulakovsky, and B. Fischer, "Complete characterization of optical pulses by real-time spectral interferometry," *Appl. Opt.*, vol. 44, no. 36, pp. 7862–7855, 2005.

[13] T.-J. Ahn, Y. Park, and J. Azaña, "Improved optical pulse characterization based on feedback-controlled Hilbert transformation temporal interferometry," *IEEE Photon. Technol. Lett.*, vol. 20, no. 7, pp. 475–477, Apr. 2008.

[14] F. Hakimi and H. Hakimi, "Measurement of optical fiber dispersion and dispersion slope using a pair of short optical pulses and Fourier transform property of dispersive medium," *Opt. Eng.*, vol. 40, no. 6, pp. 1053–1056, 2001.

[15] C. Dorrer, "Chromatic dispersion characterization by direct instantaneous frequency measurement," *Opt. Lett.*, vol. 29, pp. 204–206, 2004.

[16] G. P. Agrawal, *Nonlinear Fiber Optics*, 3rd ed. San Diego, CA: Academic, 2001, ch. 2.

[17] T. Jannson, "Real-time Fourier transformation in dispersive optical fibers," *Opt. Lett.*, vol. 8, pp. 232–234, 1983.

[18] J. Azaña and M. A. Muriel, "Real-time optical spectrum analysis based on the time-space duality in chirped fiber gratings," *IEEE J. Quantum Electron.*, vol. 36, no. 5, pp. 517–526, May 2000.

[19] M. Miyagi and S. Nishida, "Pulse spreading in a single-mode fiber due to third-order dispersion," *Appl. Opt.*, vol. 18, no. 5, pp. 678–682, 1979.
[20] I. S. Gradshteyn and I. M. Ryzhik, *Table of Integrals, Series, and Products*, 7th ed. San Diego, CA: Academic, 2007, ch. 3.69.
[21] M. Takeda, H. Ina, and S. Kobayashi, "Fourier-transform method of fringe-pattern analysis for computer-based topography and interferometry," *J. Opt. Soc. Am.*, vol. 72, no. 1, pp. 156–160, 1982.
[22] B. Costa, D. Mazzoni, M. Puleo, and E. Vezzoni, "Phase shift technique for the megsurement of chromatic dispersion in optical fibers using LED's," *IEEE J. Quantum Electron.*, vol. QE-18, no. 10, pp. 1509–1515, Oct. 1982.
[23] K. Goda, D. R. Solli, and B. Jalali, "Real-time optical reflectometry enabled by amplified dispersive Fourier transformation," *Appl. Phys. Lett.*, vol. 93, no. 3, pp. 0311061–0311063, 2008.
[24] L. Lepetit, G. Cheriaux, and M. Joffre, "Linear techniques of phase measurement by femtosecond spectral interferometry for applications in spectroscopy," *J. Opt. Soc. Am. B*, vol. 12, no. 12, pp. 2467–2474, 1995.
[25] M. Westlund, P. A. Andrekson, H. Sunnerud, J. Hansryd, and J. Li, "High performance optical-fiber-nonlinearity-based optical waveform monitoring," *J. Lightw. Technol.*, vol. 23, no. 6, pp. 2012–2022, Jun. 2005.
[26] X. Fang and R. O. Claus, "Polarization-independent all-fiber wavelength-division multiplexer based on a Sagnac interferometer," *Opt. Lett.*, vol. 20, no. 20, pp. 2146–2148, 1995.

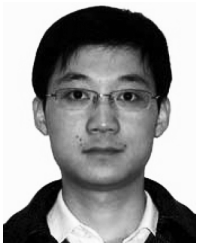

Haiyun Xia received the B.S. degree in physics and M.S. degree in optics from Soochow University, China, in 2003 and 2006, respectively. Currently, he is working toward the Ph.D. degree in optoelectronics as a joint training student in Beijing University of Aeronautics and Astronautics, China, and the University of Ottawa, Ottawa, Canada.

His current research interests include all-optical signal processing, ultrashort laser pulse characterization, laser remote sensing, and fiber-optic sensors.

Jianping Yao (M'99–SM'01) received the Ph.D. degree in electrical engineering, in 1997, from the Université de Toulon, Toulon, France.

He joined the School of Information Technology and Engineering, University of Ottawa, Ontario, Canada, in 2001, where he is currently a Professor, Director of the Microwave Photonics Research Laboratory, and Director of the Ottawa-Carleton Institute for Electrical and Computer Engineering. From 1999 to 2001, he held a faculty position with the School of Electrical and Electronic Engineering, Nanyang Technological University, Singapore. He holds a Yongqian Endowed Visiting Chair Professorship with Zhejiang University, China. He spent three months as an Invited Professor in the Institut National Polytechnique de Grenoble, France, in 2005. His research has focused on microwave photonics, which includes all-optical microwave signal processing, photonic generation of microwave, millimeter-wave and THz, radio over fiber, UWB over fiber, fiber Bragg gratings for microwave photonics applications, and optically controlled phased array antenna. His research interests also include fiber lasers, fiber-optic sensors, and biophotonics. He has authored or co-authored over 130 papers in refereed journals and over 110 papers in conference proceeding.

Dr. Yao received the 2005 International Creative Research Award of the University of Ottawa. He was the recipient of the 2007 George S. Glinski Award for Excellence in Research. He was named University Research Chair in Microwave Photonics in 2007. He was a recipient of an NSERC Discovery Accelerator Supplements award in 2008. He is an Associate Editor of the *International Journal of Microwave and Optical Technology*. He is on the Editorial Board of IEEE TRANSACTIONS ON MICROWAVE THEORY AND TECHNIQUES. He is a registered professional engineer of Ontario. He is a member of SPIE, OSA and a senior member of IEEE/LEOS and IEEE/MTT.